coatings

MDPI

Article

Relaxor Ferroelectric $AgNbO_3$ Film Fabricated on (110) $SrTiO_3$ Substrates via Pulsed Laser Deposition

Qingzhu Ma [1,2], Yao Yao [3], Dandan Su [1,*], Suwei Zhang [4,5] and Lei Zhao [2,*]

[1] College of Quality and Technical Supervision, Hebei University, Baoding 071002, China; qingzhu1232022@163.com
[2] Key Laboratory of High-Precision Computation and Application of Quantum Field Theory of Hebei Province, College of Physics Science and Technology, Hebei University, Baoding 071002, China
[3] Beijing Institute of Metrology, Beijing 100029, China; yaoy@bjjl.cn
[4] State Key Laboratory of New Ceramics and Fine Processing, School of Materials Science and Engineering, Tsinghua University, Beijing 100084, China; zhangsw999@mail.tsinghua.edu.cn
[5] Foshan (Southern China) Institute for New Materials, Foshan 528247, China
* Correspondence: sudandanhbu@hbu.edu.cn (D.S.); leizhao@hbu.edu.cn (L.Z.)

Abstract: $AgNbO_3$-based materials have attracted extensive attention in energy storage due to their double hysteresis loops, but they suffer from low breakdown strength (E_b). $AgNbO_3$ films with few defects and small thickness exhibit high E_b, which helps to improve the energy storage performance. In this work, we successfully prepared $AgNbO_3$ thin films on (110) $SrTiO_3$ substrate using pulsed laser deposition technology. The $AgNbO_3$ film shows good crystalline and relaxor ferroelectric behavior. A high E_b up to 1200 kV/cm is obtained in $AgNbO_3$ film, which contributes to good recoverable energy storage density W_{rec} up to 10.9 J/cm^3 and energy efficiency η of 75.3%. Furthermore, the W_{rec} remains above 2.9 J/cm^3 and the η varies between 72.5% and 82.5% in a wide temperature range of 30–150 °C. This work reveals the great potential of relaxor ferroelectric $AgNbO_3$ film for energy storage.

Keywords: $AgNbO_3$; film; relaxor ferroelectric; energy storage

Citation: Ma, Q.; Yao, Y.; Su, D.; Zhang, S.; Zhao, L. Relaxor Ferroelectric $AgNbO_3$ Film Fabricated on (110) $SrTiO_3$ Substrates via Pulsed Laser Deposition. *Coatings* **2023**, *13*, 1834. https://doi.org/10.3390/coatings13111834

Academic Editor: Carlos Jose Macedo Tavares

Received: 12 September 2023
Revised: 24 October 2023
Accepted: 24 October 2023
Published: 26 October 2023

1. Introduction

Dielectric capacitors with advantages of ultra-fast charge and discharge rates, excellent cycle stability, and long service life have been widely used in electric vehicles, pulse power systems and portable electronic devices [1,2]. Linear dielectrics, ferroelectric (FE) materials, antiferroelectric (AFE) materials, and relaxor ferroelectric (RFE) materials are commonly used materials in high-power capacitors. However, the energy storage density and energy efficiency of electronics capacitors are limited, and they cannot meet the requirements of miniaturization, nor can they meet the integration of advanced electrical and electronic systems. Therefore, many tasks have been performed to improve the energy storage density and energy efficiency of the capacitor [1–5].

Energy storage can be realized via dielectric polarization P in an external electric field E (P-E loops) in dielectrics, with recoverable energy storage density W_{rec} (determined by $\int_{P_r}^{P_{max}} E dP$) and energy efficiency η (defined as $W_{rec}/(W_{rec} + W_{loss})$). P_{max} and P_r are the maximum polarization and remnant polarization. P_r would generate energy loss W_{loss} and cause an energy (heat) dissipation problem in practical uses [6]. High W_{rec} and η are thus to be achieved by realizing large polarization (P_{max}) and small hysteresis (P_r and W_{loss}) [7]. In addition, the large applied electric field E, which is limited by the breakdown strength E_b, is also responsible for the high energy storage performance (ESP). AFE and REF materials with large ΔP caused by high P_{max} and small P_r are very promising for high-performance dielectric capacitors [8,9]. $AgNbO_3$-based AFE ceramics with phase transitions from M_1 phase, M_2 phase, M_3 phase, O phase, T phase to C phase have received increasing attention for energy storage because of their typical double P-E loops with high

P_{max} and low P_r [10–14]. The W_{rec} has been increased to more than 5.0 J/cm^3 via ions doping at the A- or B-site [15–17]. In addition, increasing E_b is another effective strategy to optimizing the energy storage performance of $AgNbO_3$-based ceramics, which can be realized by either regulating the preparation process or reducing the sample thickness. For example, a high E_b of 250 kV/cm is obtained in $AgNbO_3$ ceramic using hydrothermal-synthesized nano $AgNbO_3$ powders [18]. The E_b of $AgNbO_3$ ceramic reaches to 307 kV/cm by using the tape casting process, which contributes to an increased W_{rec} of 2.8 J/cm^3 [19]. It is also an effective way to enhance E_b by reducing the sample thickness since E_b follows an exponential decay relationship with the sample thickness [7]. Compared with ceramic bulks, multilayer ceramic capacitors (MLCCs) with a thin monolayer (i.e., 10–20 μm) usually contribute to high E_b and high W_{rec}. For example, an ultra-high E_b of 1500 kV/cm was obtained in $(Ag_{0.91}Sm_{0.03})(Nb_{0.80}Ta_{0.20})O_3$ MLCC with a dielectric layer of 12 μm, which contributes to an ultra-high W_{rec} of 15.0 J/cm^3 [20]. Furthermore, films with a thickness of several microns or less normally have higher E_b than their bulk counterparts. For example, $AgNbO_3$ film with a thickness of 2.6 μm shows E_b of 352 kV/cm [12]. An amount of 400 nm $AgNbO_3$ film shows an E_b of 624 kV/cm, which displays double *P*-*E* loops [13]. A further high E_b of 1200 kV/cm is obtained in 550 nm RFE $AgNbO_3$ film, which results in a W_{rec} of 10.3 J/cm^3 and a η of 72.2% [21].

It is found that the AFE or FE property of the $AgNbO_3$ films depends on the orientation direction and the applied electric field [12]. $AgNbO_3$ films deposited on (001)$SrTiO_3$ is AFE performance at the *E* of 100–350 kV/cm. On the (110)$SrTiO_3$ deposition, $AgNbO_3$ film has an AFE performance at 150 kV/cm and FE property as the *E* is higher than 200 kV/cm. The $AgNbO_3$ films deposited on (111)$SrTiO_3$ have FE property at 100–350 kV/cm [12].

In the present work, $AgNbO_3$ thin films are deposited on (110) $SrTiO_3$ substrate via pulse laser deposition. The crystal structure, the performance of the dielectric, and the performance of the ferroelectric were studied. The results show that the $AgNbO_3$ thin film has an extension and typical RFE nature which can contribute to a large ΔP. It is important to obtain a high E_b with more than 1200 kV/cm, which leads to a high W_{rec} up to 10.9 J/cm^3.

2. Experimental Procedure

Pulse laser deposition technology (PLD) was used to prepare the $AgNbO_3$ (ANO) film. First, 40 nm $SrRuO_3$ (SRO) layer was deposited on (110) $SrTiO_3$ (STO) substrate as bottom electrode through magnetic sputtering with the conditions of 700 °C, 50 W and 3 Pa. Second, 500 nm ANO film was grown on the SRO bottom electrode at a temperature of 650 °C. The laser sputtering frequency is 3 Hz and the energy density is approximately 250 mJ/cm^2. The obtained ANO film was annealed in high-purity oxygen at 550 °C for 1 h. Finally, the symmetrical SRO electrode (i.e., 40 nm, 50 W and 3 Pa) and Pt upper electrode (i.e., 40 nm, 60 W and 3 Pa) were prepared via magnetron sputtering.

The crystal structure and orientation of ANO films were detected via X-ray diffractometer (XRD, D8 Advance, Saarbruken, Germany) in which non-monochromatic Cu radiation was used. The angle range of XRD is 20~80° with a rate of 1.2°/min and a step size of 0.02°/s. Its microstructure and morphology were characterized using an atomic force microscope (AFM, MFP-3D, Asylum Research, Oxford, UK). The chemical valence of ANO films was evaluated on ESCALAB 250Xi X-ray photoelectron spectroscopy (XPS, Thermo Fisher Scientific, Oxford, UK) with the penetration depth of 4–10 nm. The relative dielectric constant and dielectric loss of ANO thin films were measured using an LCR tester (Radiant Technologies, Albuquerque, NM, USA). The frequency range of the dielectric spectrum is 10^3–10^6 Hz, and the oscillation voltage is 1 V. The ferroelectric characteristics of ANO thin films were studied using a ferroelectric tester (Precision LC II, Radiant Technologies, Albuquerque, NM, USA) at a frequency of 10^4 Hz.

3. Results and Discussion

Figure 1a shows the XRD patterns of Pt/SRO/ANO/SRO/STO heterostructure. In addition to the (*ll*0) diffraction peaks of STO substrate, the (*ll*0) diffraction peaks of ANO

film are also observed, which means good crystallization of ANO film. The insets in Figure 1a show the rocking curves of the ANO film and STO substrate. The FWHM of the ANO film and STO substrate are 0.423° and 0.168°, respectively.

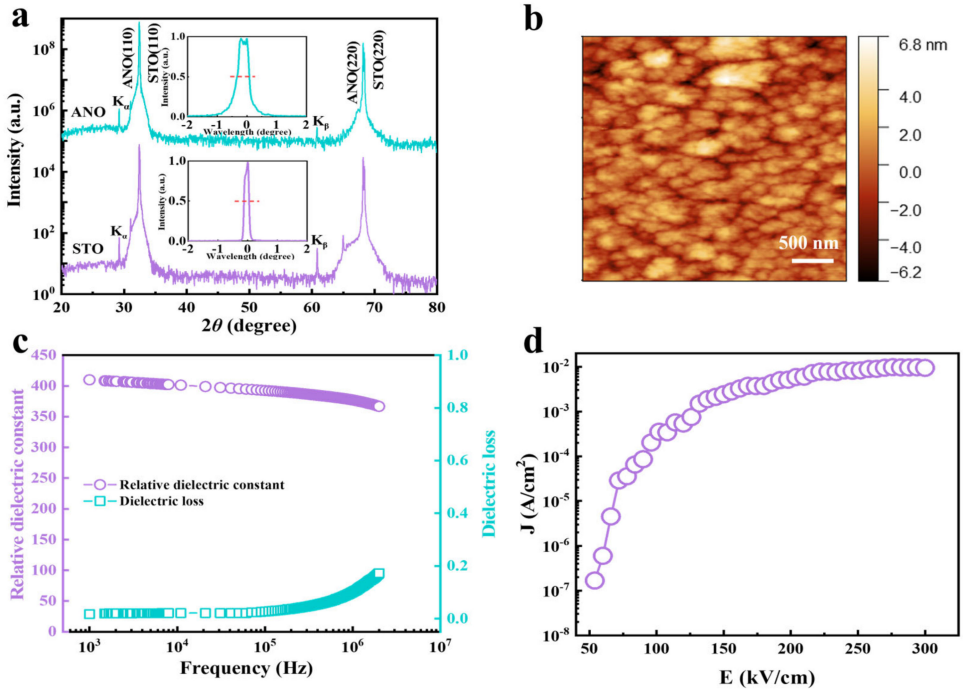

Figure 1. (**a**) XRD patterns, insets are rocking curves; (**b**) AFM image; (**c**) dielectric constant and dielectric loss as a function of frequency; (**d**) leakage current density of ANO film.

The morphology of ANO films is characterized by AFM, as shown in Figure 1b. The ANO thin films exhibit a relatively dense microstructure with root-mean-square roughness of 1.54 nm. The frequency dependence of the relative dielectric constant (ε_r) and dielectric loss (tanθ) of ANO film are shown in Figure 1c. At room temperature, ε_r and tanθ are 410 and 0.017 at 10^3 Hz in the ANO film. During the process of increasing the testing frequency from 10^3 Hz to 10^4 Hz, both ε_r and tanθ show little dependence on frequency, while ε_r decreases and tanθ increases as the frequency is greater than 10^4 Hz. The main conduction mode changes from carrier oscillation to ion oscillation at high frequency, resulting in a change in tanθ. Figure 1d shows the leakage current density of ANO film. It can be seen that the leakage current density of ANO film increased from 2.9×10^{-8} A/cm^2 to 9.4×10^{-3} A/cm^2 when E increased from 50 kV/cm to 300 kV/cm.

The chemical valence states of Ag, Nb and O elements in ANO films are investigated via the XPS spectra, as shown in Figure 2. Two peaks centered at 368.5 eV and 374.4 eV are observed in Figure 2a, which correspond to Ag $3d_{5/2}$ and Ag $3d_{3/2}$.

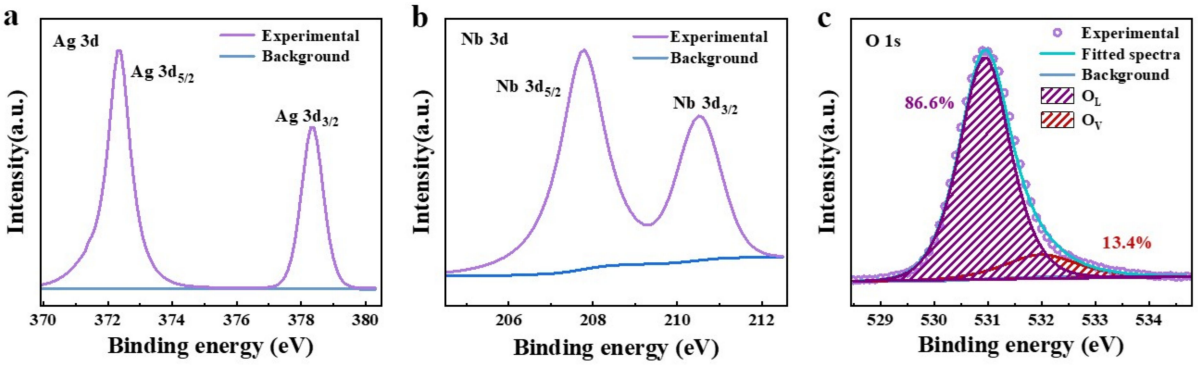

Figure 2. XPS spectra of ANO film: (**a**) Ag 3d, (**b**) Nb 3d, (**c**) O 1s.

The FWHM for Ag $3d_{5/2}$ and Ag $3d_{3/2}$ are 0.7 eV and 0.6 eV. There are two peaks centered at 210.5 eV and 208.6 eV with FWHM of 1.4 eV and 1.6 eV in Figure 2b, which correspond to Nb $3d_{5/2}$ and Nb $3d_{3/2}$. The only one spin orbit of Ag and Nb elements indicates that they have only one chemical valence state, i.e., Ag^{+} and Nb^{5+}. Therefore, it can be concluded that there is no metallic Ag in the ANO film obtained in this work. The Lorentz–Gauss function was used to perform the O 1s spectrum peak partial fitting, as shown in Figure 2c. Two peaks corresponding to oxygen vacancy (~532.0 eV, O_V) and lattice oxygen (~531.0 eV, O_L) [14] are fitted in the O 1s spectrum. The relative area of O_V is calculated to be 13.4%, which maybe the reason for the high leakage current density of ANO thin films at a higher *E*.

The *P-E* loops of the obtained ANO film were measured at a testing frequency of 10 kHz with varied *E* from 100 kV/cm to 1200 kV/cm. The results are shown in Figure 3a.

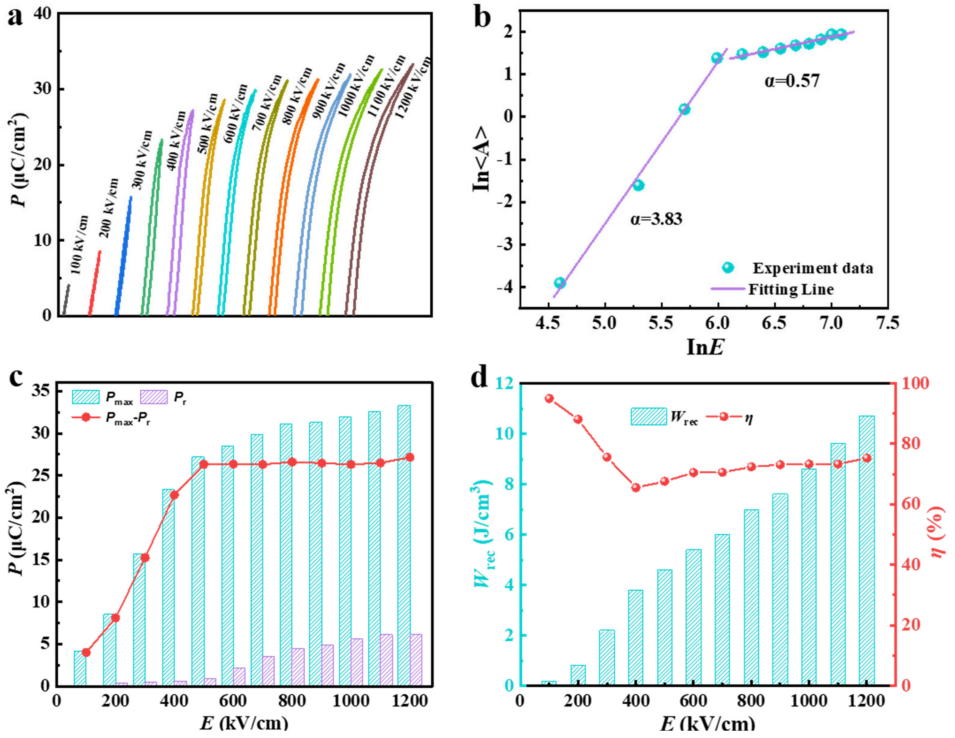

Figure 3. (**a**) *P-E* loops, (**b**) relationship between ln<A> and ln*E*, (**c**) P_{max}, P_r and ΔP, and (**d**) W_{rec} and η of ANO film at 100–1200 kV/cm.

The ANO film exhibits a slender and almost hysteresis-free *P-E* loops as *E* is less than 300 kV/cm. When *E* increases from 400 kV/cm to 1200 kV/cm, the ANO film exhibits *P-E* loops with an FE-like feature. A power law proportional relation ($<A> \propto E^{\alpha}$) is used

to produce a curve of the changes in the hysteresis area A of the ANO film with E [22], as shown in Figure 3b. Two linear stages are observed in the ln<A>-ln$E$ curve of the ANO film, indicating that the ANO film exhibits REF behavior. With the increase in E, the change in ln<A> is divided into two stages, with a rapid increase in the first stage and a slow increase in the second stage, corresponding to α values of 3.83 and 0.57, respectively. The E-induced RFE-FE state transition is the reason for the rapid increase in polarization in the first stage, and the domain growth and switching are also associated with this process [23–25]. As for the slow increase in polarization in the second stage, it may be mainly attributed to the induced polarization. At this stage, the polarization of ANO film has been nearly saturated with the increase in E, which results in small α of 0.57. The variation trends of P_r, P_{max} and ΔP ($\Delta P = P_{max} - P_r$) of the ANO thin film with E are shown in Figure 3c. Both P_r and P_{max} increases as E increases. ΔP increases rapidly as increasing E from 100 to 500 kV/cm and keeps almost unchanged as E increases from 500 to 1200 kV/cm. The increased ΔP is conducive to the improvement in ESP. When E reaches 1200 kV/cm, the P_{max}, P_r and ΔP of the ANO film are 33.3 μC/cm^2, 6.1 μC/cm^2 and 27.2 μC/cm^2, respectively. The W_{rec} and η of the ANO film are shown in Figure 3c. W_{rec} increases from 0.19 to 10.9 J/cm^3 as E increases from 100 to 1200 kV/cm. η decreases from 95.0% to 65.5% when E increases from 100 to 400 kV/cm, and gradually increases from 67.6% to 75.3% as E increases from 500 to 1200 kV/cm. Both the E_b and W_{rec} of the ANO film are much better than those of the ANO ceramics (E_b = 140–307 kV/cm and W_{rec} = 1.6–2.8 J/cm^3) prepared via the solid-state reaction method [18,19] and the pure-phase ANO film (E_b = 110 kV/cm) grown on Pt/Ti/SiO_2/Si substrate by using a chemical solution deposition method [14], but not as good as $BiFeO_3$-$BaTiO_3$-based and (Na,Bi)TiO_3-based RFE films [26,27]. High W_{rec} values of 152 J/cm^3 and 106 J/cm^3 have been obtained in the $BiFeO_3$-$BaTiO_3$-based and (Na,Bi)TiO_3-based RFE films due to their high E_b of 3500 kV/cm and 3683 kV/cm [26,27]. Therefore, if E_b can be further increased by optimizing thickness and quality, a further high W_{rec} can be expected in the ANO film.

Figure 4a shows the P-E loops of the ANO film at 30–150 °C. ANO film maintains slender P-E loops at a high temperature of 150 °C.

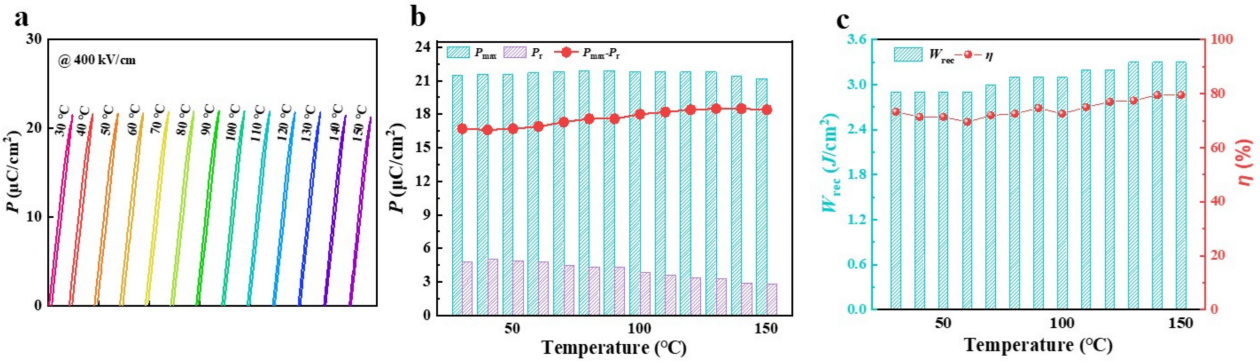

Figure 4. (**a**) P-E loops, (**b**) P_{max}, P_r, and ΔP, and (**c**) W_{rec} and η of ANO film as a function of temperature.

The changes in P_{max}, P_r and ΔP with temperature are shown in Figure 4b. Both P_r and P_{max} are found to show a decreased trend as elevating temperature from 100 °C to 150 °C. The P_r and P_{max} of the dielectric materials can be influenced by their domain wall motion, leakage current density, and phase structure [21]. Domain wall motion generally becomes easier at high temperatures, which is beneficial for high P_r and P_{max} [28]. When the temperature increases from 30 °C to 150 °C, ΔP increases from 16.7 μC/cm^2 to 18.4 μC/cm^2, which is conducive to the improvement in ESP. With the increase in temperature, W_{rec} increases from 2.9 J/cm^3 to 3.3 J/cm^3, and η varies between 72.5% and 82.5%, as shown in Figure 4c.

4. Conclusions

ANO film was fabricated on SRO/(110)STO substrate by using PLD. The ANO film has good crystalline with relatively flat surface. When E is less than 300 kV/cm, the ANO film show narrow P-E loops. When E is higher than 400 kV/cm, the P-E loops show some hysteresis. All of these conform to the RFE nature, as confirmed by the relation of $<A> \propto E^{\alpha}$. A high E_b of up to 1200 kV/cm was obtained, which contributes to a good W_{rec} of 10.9 J/cm^3 and η of 75.3% in ANO film. In addition, the W_{rec} of the ANO film remains above 2.9 J/cm^3 at 30–150 °C. This work reveals the great potential of RFE ANO film for energy storage.

Author Contributions: Conceptualization, Y.Y.; Methodology, L.Z.; Investigation, Q.M. and L.Z.; Writing—original draft, Q.M., Y.Y., D.S. and S.Z.; Writing—review & editing, S.Z. and L.Z.; Funding acquisition, L.Z. All authors have read and agreed to the published version of the manuscript.

Funding: This work was supported by the Natural Science Foundation of Hebei Province, China (No. 2021201044), the State Key Laboratory of New Ceramic and Fine Processing Tsinghua University (No. KF202005), and the Guangdong Basic and Applied Basic Research Foundation (2021A1515110185).

Institutional Review Board Statement: Not applicable.

Informed Consent Statement: Not applicable.

Data Availability Statement: Not applicable.

Conflicts of Interest: The authors declare no conflict of interest.

References

1. Li, Q.; Chen, L.; Gadinski, M.R.; Zhang, S.; Zhang, G.; Li, H.U.; Iagodkine, E.; Chen, L.Q.; Jackson, T.N. Flexible high-temperature dielectric materials from polymer nanocomposites. *Nature* **2015**, *523*, 576–579. [CrossRef] [PubMed]
2. Yao, Z.H.; Song, Z.; Hao, H.; Yu, Z.Y.; Liu, H.X. Homogeneous/inhomogeneous-structured dielectrics and their energy-storage performances. *Adv. Mater.* **2017**, *29*, 1601727. [CrossRef] [PubMed]
3. Chu, B.J.; Zhou, X.; Ren, K.L.; Neese, B.; Lin, M.R.; Wang, Q.; Bauer, F.; Zhang, Q.M. A dielectric polymer with high electric energy density and fast discharge speed. *Science* **2006**, *313*, 334–336. [CrossRef] [PubMed]
4. Pan, H.; Ma, J.; Zhang, Q.H.; Liu, X.Z.; Guan, B.; Gu, L.; Zhang, X.; Zhang, Y.J.; Li, L.L.; Shen, Y.; et al. Giant energy density and high efficiency achieved in bismuth ferrite-based film capacitors via domain engineering. *Nat. Commun.* **2018**, *9*, 1813. [CrossRef] [PubMed]
5. Peng, B.L.; Zhang, Q.; Li, X.; Sun, T.Y.; Fan, H.Q.; Ke, S.M.; Ye, M.; Wang, Y.; Lu, W.; Niu, H.B.; et al. Large energy storage density and high thermal stability in a highly textured (111)-oriented $Pb_{0.8}Ba_{0.2}ZrO_3$ relaxor thin film with the coexistence of antiferroelectric and ferroelectric phases. *ACS Appl. Mater. Interfaces* **2015**, *7*, 13512–13517. [CrossRef]
6. Li, J.L.; Shen, Z.H.; Chen, X.H.; Li, J.L.; Shen, Z.H.; Chen, X.H.; Yang, S.; Zhou, W.L.; Wang, M.W.; Wang, L.H.; et al. Grain-orientation-engineered multilayer ceramic capacitors for energy storage applications. *Nat. Mater.* **2020**, *19*, 999–1005.
7. Yang, L.T.; Kon, X.; Li, F.; Hao, H.; Cheng, Z.X.; Liu, H.X.; Li, J.F.; Zhang, S.J. Perovskite lead-free dielectrics for energy storage applications. *Prog. Mater. Sci.* **2019**, *102*, 72–108. [CrossRef]
8. Liu, X.H.; Li, Y.; Hao, X.H. Ultra-high energy-storage density and fast discharge speed of $(Pb_{0.98-x}La_{0.02}Sr_x)(Zr_{0.9}Sn_{0.1})_{0.995}O_3$ antiferroelectric ceramics prepared via the tape-casting method. *J. Mater. Chem. A* **2019**, *7*, 11858–11866. [CrossRef]
9. Peng, B.L.; Zhang, Q.; Gang, B.; Leighton, G.J.T.; Shaw, C.; Milne, S.J.; Zou, B.S.; Sun, W.H.; Huang, H.T.; Wang, Z.L. Phase-transition induced giant negative electrocaloric effect in a lead-free relaxor ferroelectric thin film. *Energy. Environ. Sci.* **2019**, *12*, 1708–1717. [CrossRef]
10. Fu, D.; Itoh, M.; Koshihara, S.Y. Dielectric, ferroelectric, and piezoelectric behaviors of $AgNbO_3$-$KNbO_3$ solid solution. *J. Appl. Phys.* **2009**, *106*, 104104. [CrossRef]
11. Yao, K.; Chen, S.T.; Rahimabady, M.; Mirshekarloo, M.S.; Yu, S.H.; Tay, F.E.H.; Sritharan, T.; Lu, L. Nonlinear dielectric thin films for high-power electric storage with energy density comparable with electrochemical supercapacitors. *IEEE. Trans. Ultrason. Ferroelectr. Freq. Control* **2011**, *58*, 1968–1974. [PubMed]
12. Sakurai, H.; Yamazoe, S.; Wada, T. Ferroelectric and antiferroelectric properties of $AgNbO_3$ films fabricated on (001), (110), and (111)$SrTiO_3$ substrates by pulsed laser deposition. *Appl. Phys. Lett.* **2010**, *97*, 042901. [CrossRef]
13. Zhang, Y.L.; Li, X.B.; Song, J.M.; Zhang, S.W.; Wang, J.; Dai, X.H.; Liu, B.T.; Dong, G.Y.; Zhao, L. $AgNbO_3$ antiferroelectric film with high energy storage performance. *J. Mater.* **2021**, *7*, 1294–1300. [CrossRef]
14. Shu, L.; Zhang, X.; Li, W.; Gao, J.; Wang, H.L.; Huang, Y.; Cheng, Y.Y.S.; Li, Q.; Liu, L.S.; Li, J.F. Phase-pure antiferroelectric $AgNbO_3$ films on Si substrates: Chemical solution deposition and phase transitions. *J. Mater. Chem. A* **2022**, *10*, 12632–12642. [CrossRef]

15. Luo, N.N.; Han, K.; Zhuo, F.P.; Liu, L.J.; Chen, X.Y.; Peng, B.L.; Wang, X.P.; Feng, Q.; Wei, Y.Z. Design for high energy storage density and temperature-insensitive lead-free antiferroelectric ceramics. *J. Mater. Chem. A.* **2019**, *7*, 14118–14128. [CrossRef]
16. Ma, L.; Che, Z.Y.; Xu, C.; Cen, Z.Y.; Feng, Q.; Chen, X.Y.; Toyohisa, F.; Li, J.-F.; Zhang, S.J.; Luo, N.N. High energy storage density and efficiency in $AgNbO_3$ based relaxor antiferroelectrics with reduced silver content. *J. Eur. Cream. Soc.* **2023**, *43*, 3228–3235. [CrossRef]
17. Zhou, J.; Du, J.H.; Chen, L.M.; Li, Y.; Xu, L.Z.; Zhao, Q.R.; Yang, H.L.; Ding, J.X.; Sun, Z.M.; Hao, X.H.; et al. Enhanced the energy storage performance in $AgNbO_3$-based antiferroelectric ceramics via manipulation of oxygen vacancy. *J. Eur. Ceram. Soc.* **2023**, *43*, 6059–6068. [CrossRef]
18. Wang, J.; Wan, X.H.; Rao, Y.; Zhao, L.; Zhu, K.J. Hydrothermal synthesized $AgNbO_3$ powders: Leading to greatly improved electric breakdown strength in ceramics. *J. Eur. Ceram. Soc.* **2020**, *40*, 5589–5596. [CrossRef]
19. Zhao, M.Y.; Wang, J.; Chen, L.; Yuan, H.; Zhang, M.H. Enhanced breakdown strength and energy storage density of $AgNbO_3$ ceramics via casting. *Rare Met.* **2023**, *42*, 495–502. [CrossRef]
20. Zhao, M.Y.; Wang, J.; Zhang, J.; Zhu, L.F.; Zhao, L. Ultrahigh energy storage performance realized in $AgNbO_3$-based antiferroelectric materials via multiscale engineering. *J. Adv. Ceram.* **2023**, *12*, 1166–1177. [CrossRef]
21. Li, X.; Wang, J.; San, X.Y.; Wang, N.; Zhao, L. High energy storage performance in $AgNbO_3$ relaxor ferroelectric films induced by nanopillar structure. *J. Mater. Sci. Technol.* **2023**, *155*, 160–166. [CrossRef]
22. Xie, A.W.; Fu, J.; Zuo, R.Z.; Jiang, X.W.; Li, T.Y.; Fu, Z.Q.; Yin, Y.W.; Li, X.G.; Zhang, S.J. Achieving stable relaxor antiferroelectric P phase in $NaNbO_3$-based lead-free ceramics for energy-storage applications. *Adv. Mater.* **2022**, *34*, 2204356. [CrossRef]
23. Yu, G.; Dong, X.L.; Wang, G.S.; Gao, F.; Chen, X.F.; Nie, H.C. Three-stage evolution of dynamic hysteresis scaling behavior in $63PbTiO_3$-$37BiScO_3$ bulk ceramic. *J. Appl. Phys.* **2010**, *107*, 106102. [CrossRef]
24. Yimnirun, R.; Wongmaneerung, R.; Wongsaenmai, S.; Ngamjarurojana, A.; Ananta, S.; Laosiritaworn, Y. Temperature scaling of dynamic hysteresis in soft lead zirconate titanate bulk ceramic. *Appl. Phys. Lett.* **2007**, *90*, 112908. [CrossRef]
25. Shi, J.P.; Chen, X.L.; Li, X.; Sun, J.; Sun, C.C.; Pang, F.H.; Zhou, H.F. Realizing ultrahigh recoverable energy density and superior charge-discharge performance in $NaNbO_3$-based lead-free ceramics via a local random field strategy. *J. Mater. Chem. C* **2020**, *8*, 3784–3794. [CrossRef]
26. Pan, H.; Lan, S.; Xu, S.Q.; Zhang, Q.H.; Yao, H.B.; Liu, Y.Q.; Meng, F.Q.; Guo, E.J.; Gu, L.; Lin, Y.-H. Ultrahigh energy storage in superparaelectric relaxor ferroelectrics. *Science* **2021**, *374*, 100–104. [CrossRef] [PubMed]
27. Tang, Z.H.; Zhou, Y.P.; Jiang, N.; Guo, F.; Chen, J.Y.; Yang, B.; Zhao, S.F. Leakage-limitation engineering derived from an interfacial charge barrier for dielectric energy storage in relaxation ferroelectric films. *J. Phys. Chem. C* **2023**, *127*, 15078–15086. [CrossRef]
28. Sciau, P.; Kania, A.; Dkhil, B.; Suard, E.; Ratuszna, A. Structural investigation of $AgNbO_3$ phases using x-ray and neutron diffraction. *J. Phys. Condens. Matter* **2004**, *16*, 2795–2810. [CrossRef]